

## **Interferometers with Internal and External Phase Modulation: Experimental and Analytical Comparison\***

*Andrew J. Stevenson, Malcolm B. Gray, Charles C. Harb, David E. McClelland  
and Hans-A. Bachor*

Department of Physics and Theoretical Physics, Faculty of Science,  
Australian National University, Canberra, ACT 0200, Australia.

### *Abstract*

Optical intensity noise in a light source easily degrades the sensitivity of a shot-noise-limited interferometer which is directly detecting low frequency phase or displacement variations. In this paper we describe and compare two experimental methods in which we use high frequency optical phase modulation to shift low frequency phase signals in an interferometer to a shot noise limited region of the photocurrent spectrum. This phase modulation is applied either within the interferometer arms—*internal modulation*—or in a local oscillator beam tapped off the main interferometer and coherently recombined with the interferometer output—*external modulation*. The photocurrent is mixed electronically with the high frequency modulating waveform to extract the signal information free from laser intensity noise. In our experiments, we have been able to detect interferometrically low frequency signals with true shot-noise-limited sensitivity. We find, theoretically and experimentally, that the interferometric sensitivity achievable in each scheme depends critically on non-ideal factors, such as imperfect interferometric fringe contrast and electronic noise in the detectors or amplifiers. This paper examines the relative merits and operating requirements of both modulation schemes in practical interferometers.

### **1. Introduction**

Optical interferometry has long been recognised (e.g. Michelson and Morley 1887) as one of the most effective methods to obtain measurements of displacement and other optical path length variations in a medium accurate to a small fraction of an optical wavelength. In recent years, the quest to detect gravitational radiation using large-scale Michelson interferometers (Weiss 1972; Hough *et al.* 1989; Sandeman and McClelland 1990; Vogt 1991; Brillet *et al.* 1992) is pushing the technology of optical phase detection to new realms of sensitivity.

The simplest and most widely implemented scheme of two-beam interferometry is known as *direct detection* (photon counting): Differential phase variations between the two light beams interfering at the final beam combiner, caused by movements of the mirrors for example, are sensed *directly* via changes in photocurrent caused by intensity variations induced in either or both of the output beams (Born and Wolf 1980).

The inherent sensitivity of an interferometer is determined by its achievable signal-to-noise ratio. We may define the *phase sensitivity* of a given interferometer at a particular signal frequency as *the minimum phase oscillation amplitude at*

\* Refereed paper based on a contribution to the inaugural Australian General Relativity Workshop held at the Australian National University, Canberra, in September 1994.

that frequency capable of producing a signal-to-noise ratio of unity at the output. The signal-to-noise ratio depends in turn on the response of the interferometer to phase variations between the interfering beams, and on the nature and magnitude of the optical noise in the interferometer at the signal frequency.

The ultimate limit to the phase sensitivity of an interferometer in the direct detection scheme is set by the Heisenberg Uncertainty Principle. Quantum mechanical noise manifests itself in two ways in an interferometer (Caves 1980, 1981; Loudon 1981): Fluctuations in the number of photons emerging from the instrument (photon counting error), and radiation pressure-induced fluctuations on mechanical components of the device (radiation pressure error). At currently available laser powers, the radiation pressure error is negligible, and the photon-counting error limits the phase sensitivity of an ideal interferometer in practice.

While a rigorous quantum mechanical treatment is required to describe fully the origins and manifestations of quantum noise in an interferometer, it turns out that a simple phenomenological model of the photon counting error is sufficient for our purposes, and provides the same basic sensitivity predictions. In the analysis to be described in this paper, the photon counting error appears as 'shot noise', a Poissonian statistical variation in the photocurrent which scales in proportion to the square root of the detected light intensity, and which possesses a flat noise spectrum (Bachor and Fisk 1989; Bachor and Manson 1990). Over most of the frequency spectrum, this is an accurate description applicable to interferometers operated with lasers, LEDs or bright incandescent sources. Interferometers operated with 'squeezed states' of light (Caves 1981; Gea-Banacloche and Leuchs 1986, 1987; Xiao *et al.* 1987) require a detailed quantum mechanical analysis to predict their sensitivity, and will not be considered in this paper.

The large photon number flux generally detected in an interferometric measurement ensures that shot noise fluctuations are very small compared to the DC photocurrent. If all other sources of noise in the interferometer are made negligible (not a straightforward task), true shot-noise-limited interferometry becomes possible, permitting *extremely fine phase resolution*.

Operating with quantum-noise-limited sensitivity also achieves an *intensity-scaling advantage*: Increasing the input light intensity increases signals proportionally, but shot noise only increases as the square root of the input intensity, so the shot-noise-limited phase sensitivity improves as the inverse square root of the input intensity. It may not be possible to exploit direct increases in the input intensity due to limited power available from the light source, but the intensity-scaling advantage just described may be realised through the use of 'optical recycling' techniques (Drever 1983; Meers 1988; Vinet *et al.* 1988; Strain and Meers 1991; Fritschel *et al.* 1992) which effectively boost the input power by using a mirror to return to the interferometer light otherwise wasted at an unused output port.

Shot noise is not the only optical noise contribution in interferometric sensors, generally. Most light sources used in interferometry exhibit intensity fluctuations, particularly at low frequencies, known as *technical noise* (or alternatively *classical noise* or *relative intensity noise*). This type of noise appears just like a signal in the photocurrent, in direct proportion to the detected light level, so the intensity-scaling advantage just described is lost at signal frequencies where technical noise dominates.

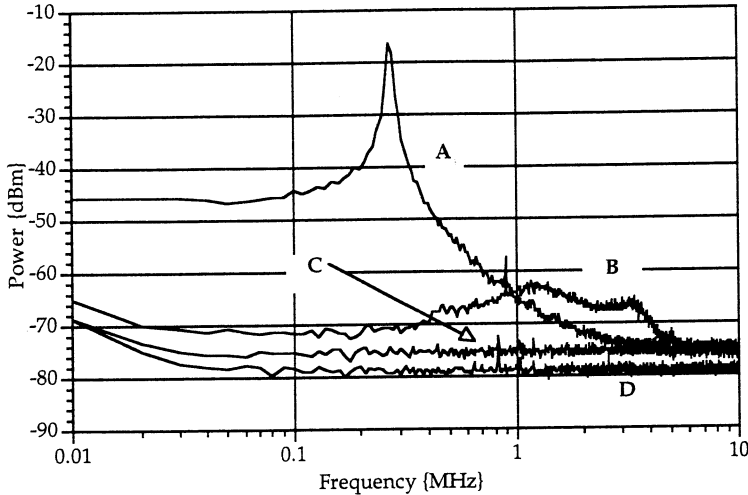


**Fig. 1.** Typical laser intensity noise spectra obtained from a Nd:YAG non-planar ring laser ('MISER') with 17.5 mW of optical power detected on a standard InGaAs detector: A, the intensity noise output of the free running laser system; B, the intensity noise output with opto-electronic feedback control; C, the standard shot noise floor for identical photocurrent and receiver bandwidth as used in A and B, obtained with a quiet incandescent source (some electronic detector noise is evident at frequencies below 0.1 MHz); and D, the electronic noise floor of the detection system with no light on the detector. (Reproduced with permission from Harb *et al.* 1994.)

Technical noise is either narrowband or broadband in nature, but tends to be more prominent at low frequencies where it may be orders of magnitude greater than the shot noise. In particular, many solid state lasers exhibit a very strong relaxation oscillation at low frequencies, driven by random internal processes (Yariv 1985). Measurable intensity fluctuations may persist at low frequencies in spite of elaborate measures taken to stabilise the source (Robertson *et al.* 1986; Kane 1990; Hough *et al.* 1991; Harb 1991; Tsubono and Moriwaki 1992; Rowan *et al.* 1994). Fig. 1 (Harb *et al.* 1994) shows photocurrent noise spectra obtained from a diode-pumped Nd:YAG non-planar ring laser operating at around 17.5 mW, running free and running with feedback stabilisation, compared to the shot noise spectrum associated with the same average photocurrent. Below a few MHz, the relaxation oscillation dominates the flat shot noise floor in the free-running laser. Even with intensity stabilisation active, the residual technical noise still dominates shot noise out to at least 5 MHz.

The standard technique to overcome technical noise in the direct detection scheme is by common-mode cancellation: The interferometer is operated exactly midway between the bright and dark fringes, both output ports of the final beam combiner are detected and one photocurrent is subtracted from the other. Technical noise from the light source, being common to both outputs (correlated), is cancelled. Differential phase signals in the interferometer produce intensity variations out of phase (anticorrelated) at each detector, and are recovered by the subtraction process. Shot noise, however, is completely uncorrelated at the two outputs for quantum mechanical reasons and is therefore not susceptible to common-mode cancellation.

When shot noise is taken into account in the direct detection scheme, the balanced detector operating condition is no longer found to be optimal. Rather, setting the interferometer very closely to a dark fringe and detecting only that output results in the optimum sensitivity in the limit of the ideal interferometer. While this may appear paradoxical, we have already shown analytically and experimentally (Stevenson *et al.* 1993) that operating near the dark fringe minimises technical noise, shot noise and signals in such a way that the signal-to-noise ratio is maximised. In a direct detection demonstration, we were thus able to achieve shot-noise-limited sensitivity using a reflective polarimeter to sense electric and magnetic fields.

Direct detection interferometry reveals a serious drawback when unrelated noise is present, for example, electronic noise in the detector and amplifiers, or unwanted shot noise due to transmission of light at imperfect dark fringes. To optimise the signal-to-noise ratio in the presence of unrelated noise, it is necessary to detune the interferometer significantly from the dark fringe condition. The resulting extra optical transmission reintroduces technical noise from the light source, which can prevent shot-noise-limited measurements at low frequencies.

*Phase modulation interferometry* is a useful technique to circumvent this technical noise problem encountered in direct detection interferometry and achieve true shot-noise-limited phase sensitivity at low signal frequencies. The basic scheme is to impose high frequency phase or frequency modulation on the light, either within or outside the interferometer, to frequency-shift the phase signals from low frequencies into a shot-noise-limited region of the photocurrent spectrum. This has the side-effect of frequency-shifting the technical noise also. Because the technical noise is correlated in each beam while signal information is anticorrelated, operating the interferometer exactly on a dark fringe cancels optically the frequency-shifted technical noise while retaining the frequency-shifted signal information. The baseband signal information is extracted or 'demodulated' by multiplying the resulting photocurrent with the original modulating waveform and low pass filtering to remove higher harmonics. Dark fringe operation has three important effects in phase modulation interferometry:

- (i) the demodulated signal is maximised;
- (ii) the demodulated technical noise is suppressed; and
- (iii) the shot noise is minimised.

In recent years, phase modulation techniques have received attention in a variety of interferometric sensing applications ranging from microscopic surface profiling (Sasaki and Okazaki 1986), electric and magnetic field measurements (Heinrich *et al.* 1986; Weigarten *et al.* 1988; Stevenson *et al.* 1993) and displacement measurements (Yoshino *et al.* 1987). In this paper we discuss two particular RF modulation techniques, *internal modulation* and *external modulation* (Weiss 1972; Hello 1990; Man *et al.* 1990; Strain 1991; Fritschel 1991; Stevenson *et al.* 1993), which have been investigated for their potential use in interferometric gravity wave detection, and can be usefully employed in other interferometric sensing applications to overcome the effects of technical noise in light sources and enable shot-noise-limited interferometry. The primary objective of this paper is to inform other potential users of high-sensitivity interferometry about these useful new techniques.

In recent experiments in our own laboratories (Stevenson *et al.* 1993; Gray *et al.* 1995), we have successfully demonstrated that both the internal and external modulation schemes are capable of suppressing technical noise from the light source by many orders of magnitude. Recently, using external modulation in conjunction with a Michelson interferometer, we achieved true shot-noise-limited sensitivity at frequencies where technical noise completely dominates the direct detection photocurrent spectrum.

In part, this paper reviews the material covered in Stevenson *et al.* (1993) and Gray *et al.* (1995), with a view to comparing the two modulation schemes theoretically and experimentally. In Section 2 we describe the generic internal and external modulation configurations used in our analytic models, and compare their inherent sensitivities when non-ideal practical considerations, such as imperfect interferometric fringes and electronic detector noise, are taken into account. Section 3 describes our benchtop experiments which we performed to verify our simple analytic models of phase modulated interferometers, and outlines some important practical implications of these experiments. We discuss in Section 4 some broader issues which may affect the choice of scheme to be used in practice, and in Section 5 we present our conclusions.

## **2. Internal and External Modulation Interferometry: Physical Description and Analytic Results**

### *(2a) Internal and External Modulation Configurations*

The two generic modulation schemes to be compared here apply also to other interferometric configurations (e.g. Mach-Zehnder, Polarimeter, etc.) but here, for illustration, we consider mainly the Michelson configuration. The measured 'signal' is a differential phase variation or optical path difference between two arms induced by any mechanism or transducer (e.g. mirror displacement changes, refractive index or birefringence changes in an electro-optic crystal etc.).

*Internal modulation:* Electro-optic crystals (Pockels Cells) phase modulate the light within one or both interferometer arms, superimposing a high-frequency oscillation in the differential phase on the existing low-frequency differential phase signal. A broadband photodetector senses both slow (baseband or signal) variations and fast (modulation frequency) oscillations in the intensity at the output. Fig. 2 shows the generic configuration for the internal modulation scheme.

*External modulation:* This configuration separates the tasks of signal and high-frequency phase modulation into two locations. The Michelson interferometer hosts the low-frequency differential phase signals again, but in this scheme, the electro-optic crystal imposes its high-frequency phase modulation onto a local oscillator beam, tapped off a convenient beam in the system (e.g. the Michelson input beam). A second beam combiner coherently superimposes the rapidly modulated local oscillator beam and slowly modulated Michelson output beam onto a pair of detectors. This constitutes a Michelson interferometer within a Mach-Zehnder interferometer. Fig. 3 shows the generic external modulation arrangement.

We now consider each modulation configuration to illustrate how the low-frequency signal of interest is shifted into the high-frequency regime and subsequently demodulated.

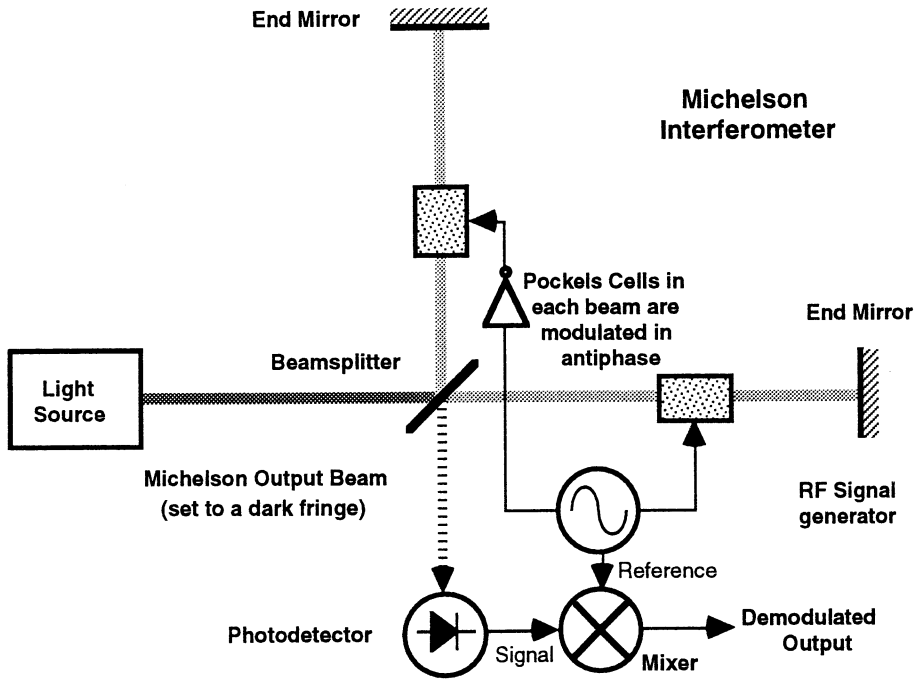


Fig. 2. Generic internal modulation configuration described in this paper.

### (2b) Signal Extraction in the Internal Modulation Scheme

Consider the basic Michelson interferometer in both of the modulation schemes of Fig. 2 and Fig. 3. The end mirrors exhibit an average reflectivity of  $R$ , say, where  $0 \leq R \leq 1$ , and the interferometer is characterised by a fringe 'visibility'  $V = (P_{\max} - P_{\min}) / (P_{\max} + P_{\min})$ , where  $P_{\max}$  and  $P_{\min}$  are the maximum and minimum detected output powers at the bright and dark fringes respectively (note:  $0 \leq V \leq 1$  always). Visibility below unity indicates that the interferometer is 'non-ideal', in that it still transmits some light at its 'dark fringe' condition. The output power from the interferometer varies with the total instantaneous optical phase difference  $\theta(t)$  between the two beams, as measured at the output, and without loss of generality, we may write this output power as

$$P_{\text{out}} = P_{\text{in}} R [1 + V \cos \theta(t)] / 2, \quad (1)$$

where  $P_{\text{in}}$  is the effective input light power. In the internal modulation configuration, the total optical phase difference between the two arms is simply the sum of the DC phase setting  $\theta_0$  due to static arm length differences etc., the signal phase  $\theta_s(t)$  due to the quantity being sensed, and a high-frequency phase variation  $\theta_m(t)$  due to the modulation in the arms. We may then write

$$\theta(t) = \theta_0 + \theta_s \sin(\omega_s t + \chi_s) + \theta_m \sin(\omega_m t + \chi_m). \quad (2)$$

Here  $\theta_s$  and  $\theta_m$  are the phase modulation depths for the signal and high-frequency modulations at frequencies  $\omega_s$  and  $\omega_m$  respectively, and  $\chi_s$  and  $\chi_m$  represent phase offsets of the signal and modulation waveforms. In the external modulation scheme, the second modulation term  $\theta_m(t)$  is absent in the Michelson.

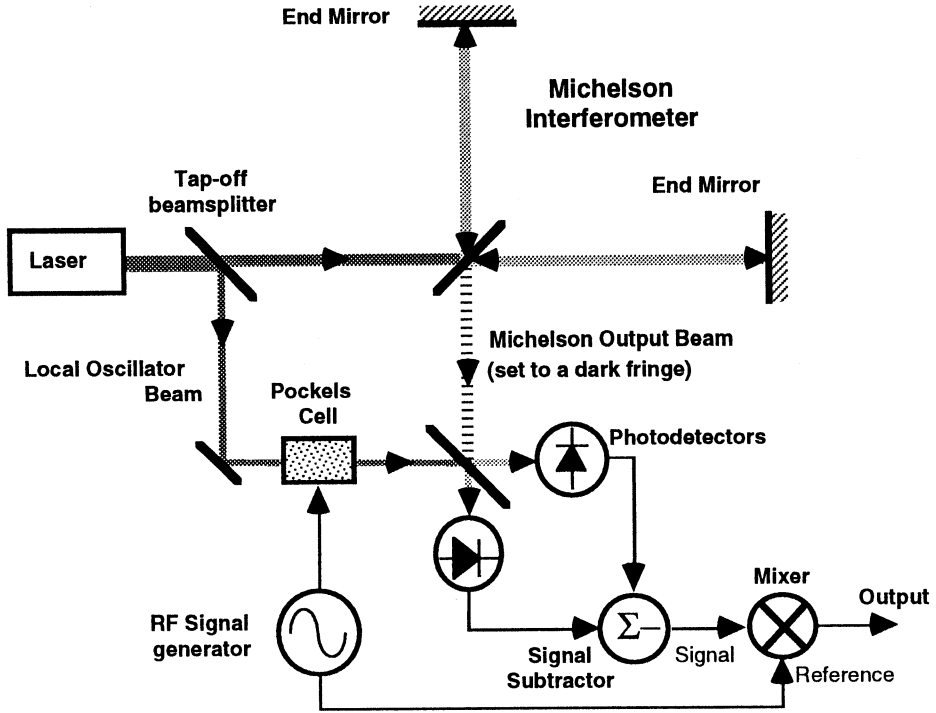
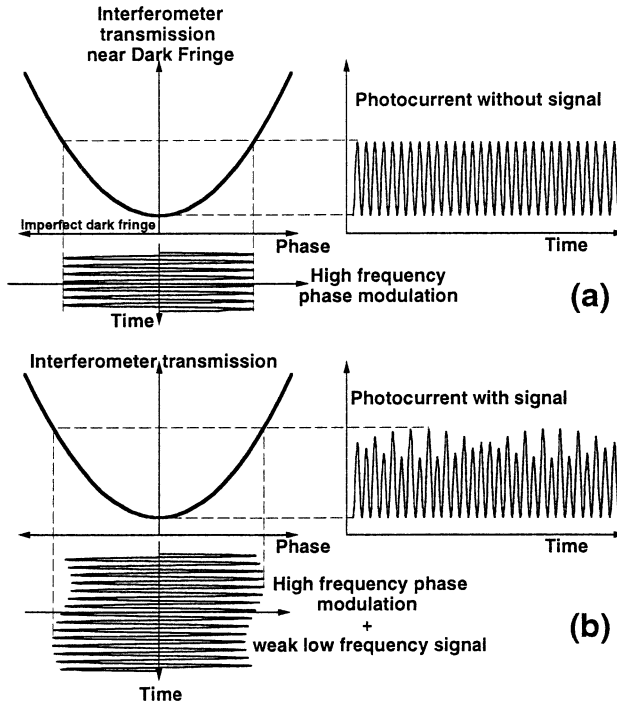


Fig. 3. Generic external modulation configuration described in this paper.

The internal modulation system feeds the Michelson output directly to a detector which produces a photocurrent  $i(t) = \rho P(t)$ , say, where  $\rho$  is the detector responsivity (usually expressed in Amps per Watt). The phase expression (2) can be inserted into the interferometer output power equation (1). A standard harmonic expansion of  $\cos\theta(t)$ , performed using Bessel function coefficients shows that this photocurrent contains a DC component, and oscillatory components at the signal and modulation frequencies, as well as higher harmonics of each, and also components at the sum and difference frequencies  $\omega_s \pm \omega_m$ . Each term varies with the DC phase setting  $\theta_0$ . Rather than detail this expansion and subsequent analysis, it is perhaps more illustrative to consider some schematic plots of the time-dependent output current from this device, as shown in Fig. 4.

When the high-frequency modulation is relatively strong, the second harmonic of the modulation frequency ( $2\omega_m$ ) dominates the photocurrent when the interferometer is set to a dark fringe since the output of the interferometer varies quadratically with phase at that point. Fig. 4a shows this component in the absence of any applied low-frequency signal. Because its amplitude varies only weakly near the dark fringe, this harmonic conveys little or no information regarding the instantaneous magnitude or sign of the low-frequency signal.



**Fig. 4.** Waveforms obtained in the internal modulation scheme: (a) High-frequency sinusoidal phase modulation about the dark fringe condition leads to a constant amplitude second harmonic appearing in the photocurrent. (b) A low-frequency phase signal superimposed on the high-frequency internal modulation in the interferometer produces a corresponding asymmetry in the photocurrent waveform.

Adding a low-frequency phase signal to the high-frequency phase modulation in the interferometer introduces into the waveform of Fig. 4b a measurable *asymmetry*, whose magnitude and parity tracks the instantaneous signal at frequency  $\omega_s$ . This type of asymmetry, in which subsequent peaks of the waveform alternate in height, indicates the existence of components at or near the fundamental modulation frequency  $\omega_m$ . In this case, the sinusoidal time variation of the asymmetry around the symmetric waveform condition indicates the presence of sum and difference frequencies  $\omega_s \pm \omega_m$  in the waveform. These sidebands contain the frequency shifted signal information we seek to recover. In fact, in the example shown in Fig. 4b, there is no component present in the output of the interferometer at the fundamental modulation frequency  $\omega_m$ .

We extract baseband signal information by multiplying or ‘mixing’ the AC components of the output waveform with the fundamental modulation waveform, to ‘pick out’ the fundamental harmonic and nearby frequencies. Low-pass filtering (integrating) the resulting waveform yields the required signal information. Fig. 5 shows both the complicated mixer output waveform and the low-pass filtered result. A symmetric input (second modulation harmonic only) to the mixer would yield a flat ‘zero signal’ output after filtering.

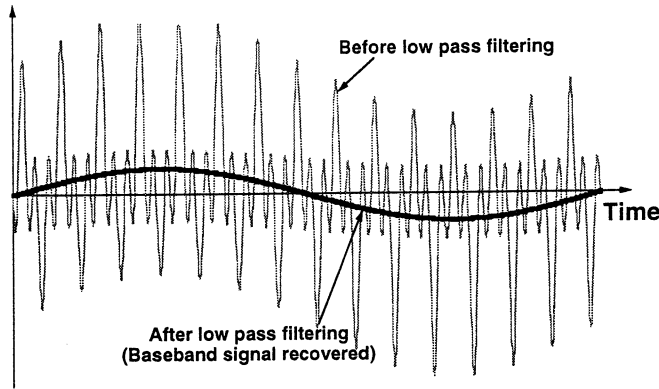


**Fig. 5.** Electronically mixing the asymmetric photocurrent waveform of Fig. 4b with the original high-frequency modulation waveform produces a complex waveform (light shading) containing several modulation harmonics. Low-pass filtering reveals the original baseband signal waveform.

### (2c) Demodulated Noise in the Internal Modulation Scheme

An important question must be asked: What happens to the laser intensity noise after this modulation and demodulation process? In other words, will the laser intensity noise appear in the demodulated output?

To survive the demodulation process and appear as an output variation at some frequency  $\omega_{\text{noise}}$ , there must exist a component in the interferometer output at frequency  $\omega_m \pm \omega_{\text{noise}}$ . This would show up as another time varying asymmetry with an envelope frequency of  $\omega_{\text{noise}}$ , just as the signal did in Fig. 4b. To create an asymmetry of this nature in the interferometer output waveform when the interferometer is set to a dark fringe, there must be some differential phase noise  $\theta_{\text{noise}}(t)$  within the interferometer at that frequency, just as a differential phase signal at frequency  $\omega_s$  was required to create an output at frequency  $\omega_m \pm \omega_s$ . Clearly, *input intensity noise* is not the same thing as *interferometric phase noise*. In fact, the intensity noise can only fractionally modulate the *height* of the entire waveform, so at most, it appears on the output signal as a small fractional modulation of that signal. This means that operation at the dark fringe has simultaneously *maximised the observed signal* and *minimised the observed noise* in the demodulated output of the system.

In summary then, the key to the simultaneous suppression of input intensity noise and maximisation of the interferometric phase signal in the final demodulated output is to exploit *waveform symmetry near a dark fringe*: The phase signal within the interferometer affects the symmetry of the interferometer output waveform, in both magnitude and parity, while intensity noise is not able to do this.

It is not possible, of course, to maintain a practical interferometer *exactly* at any fixed phase condition, due to vibrations in the interferometer or frequency noise in the light source, for example. Minute deviations from the dark fringe reintroduce the first harmonic of the modulation frequency. Intensity noise will modulate the amplitude of this harmonic as it modulates the entire waveform.

The resulting fluctuations will appear now in the demodulated output and can easily dominate shot noise and comparable signals at low frequencies, even for small phase deviations from the dark fringe. The rms phase deviations from the dark fringe may be made extremely small by the use of high gain servo loops which compensate the vibrations to lock the interferometer phase. As the phase deviations are reduced, the residual noise decreases, and it is possible to operate at lower frequencies with shot-noise-limited sensitivity.

It might be asked: Why not lock the interferometer to the midpoint between the bright and dark fringes, and demodulate instead using the *second* harmonic of the high-frequency modulation, at frequency  $2\omega_m$ ? It is certainly true that the signal information can be obtained this way, but the frequency shifted components at frequencies  $2\omega_m \pm \omega_s$  have smaller amplitudes [proportional to  $J_2(\theta_m)$  instead of  $J_1(\theta_m)$ ], and more importantly, the extra light detected leads to much greater shot noise.

*(2d) Optimising Sensitivity in the Internal Modulation Scheme*

This brings us to the final point of interest: If the technical noise from the laser is properly suppressed by tuning to a dark fringe, can the signal-to-shot-noise ratio be optimised further in any way?

To answer this question, it must first be recognised that in any practical interferometer, laser intensity noise is not the only type of noise which degrades sensitivity. There are always two other principal sources of noise in any real system which must always be addressed if shot-noise-limited operation is required:

- (i) electronic noise in the detectors and amplifiers, and
- (ii) extra shot noise due to imperfect fringe contrast in the Michelson.

Even after the interferometer and detection electronics are optimised, these two noise sources will remain at some level, capable of obscuring small signals, unless steps are taken to compensate for them. Other noise sources, such as beam pointing noise, vibrations in optical components etc., are not universal, so for simplicity and clarity these will not be treated here.

In the internal modulation scheme, the chief degree of freedom, apart from the DC phase setting  $\theta_0$  of the Michelson interferometer, is the high-frequency phase modulation depth  $\theta_m$ . The larger the modulation depth, the stronger is the demodulated signal—this appears to be the best available method for increasing signal strength to overcome unwanted noise. However, the modulation itself drives the interferometer away from the dark fringe twice in each cycle, leading to extra optical transmission and hence further shot noise. A trade-off exists, therefore between signal strength, unwanted electronic and shot noise and extra modulation-induced shot noise, and there is an optimum modulation depth required to maximise the signal-to-noise ratio. A careful analysis is needed to calculate this optimum  $\theta_m$  for the given level of background noise.

It turns out that the signal amplitude varies in proportion to  $J_1(\theta_m)$  where  $\theta_m$  is the modulation depth while the rms shot noise amplitude varies like  $\sqrt{[1 - VJ_0(\theta_s)J_0(\theta_m) + VJ_0(\theta_s)J_2(\theta_m)]}$ . The first two terms inside the  $\sqrt{\quad}$  sign relate to the demodulated shot noise associated with the average DC intensity at the detector—a combination of residual dark fringe transmission and unavoidable modulation-induced average transmission.

The origin of the third term is not so obvious—it is a correction arising from the demodulation of ‘non-stationary’ shot noise (Meers and Strain 1991; Niebauer *et al.* 1991; Mio and Tsubono 1992; Gray *et al.* 1993). The sinusoidal demodulating waveform varies in step with the time-varying shot noise associated with the oscillating light intensity at the detector. Synchronous demodulation of the varying noise leads to an overestimate of the shot noise by up to 50% (worst when the output light is fully intensity modulated, i.e. when the interferometer produces perfect dark fringes). It is not possible to avoid this penalty by the use of the other demodulating quadrature (i.e. by demodulating with a wave 90° out of phase with the shot noise variation), because that would not demodulate any signal whatsoever. The optimum demodulating phase is still the one which maximises the demodulated signal.

After a detailed analysis of the internal modulation system, it can be shown that the ratio of signal power to total noise power measured by a phase insensitive receiver at the demodulator output is given by

$$S/N = \frac{(\rho P_{\text{in}}/eB)RV^2 J_1^2(\theta_s) J_1^2(\theta_m)}{1 + 2\epsilon - V J_0(\theta_s) J_0(\theta_m) + V J_0(\theta_s) J_2(\theta_m)}, \quad (3)$$

where  $\rho$  is the detector responsivity,  $P_{\text{in}}$  is the input power,  $B$  is the resolution bandwidth,  $e$  is the fundamental electronic charge ( $1.6 \times 10^{-19}$  C),  $R$  is the average end mirror reflectivity,  $V$  is the interferometric fringe visibility,  $J_0$ ,  $J_1$  and  $J_2$  are Bessel functions of the first kind,  $\theta_s$  and  $\theta_m$  are the phase modulation depths for the signal and high-frequency phase modulation respectively, and  $\epsilon$  is a normalised electronic noise factor, given by the ratio of broad band electronic noise power seen at the receiver to the demodulated shot noise power which would be observed in the same bandwidth if all of the input light was incident on the detector.

Equation (3) assumes that dark fringe operation has been arranged and that the only reason for imperfect dark fringes is mismatched mirror reflectivities in the Michelson (i.e. perfect beam matching has been assumed in the derivation for simplicity). Equation (3) also assumes that the optimal demodulating waveform quadrature is used. The interferometer can be regarded as ‘shot noise limited’ when the  $2\epsilon$  factor in the denominator is negligible compared to the remaining terms, but some of the shot noise is due to unwanted transmission from the imperfect dark fringe.

It is worth noting that the shot noise power due to a simple DC photocurrent of magnitude  $i_{\text{DC}}$  at a detector, and measured in a bandwidth  $B$  by a receiver with input impedance  $R$ , is given by

$$\text{Shot noise power} = \langle i_{\text{shot}}^2 \rangle R = 2ei_{\text{DC}} BR. \quad (4)$$

This is extremely small, even if a high gain amplifier is inserted between the detector and the receiver. For example, if a detector photocurrent of 10 mA is impedance matched into a broadband amplifier with 60 dB gain, and from there to matched receiver, the shot noise power is only  $\sim 10^{-10}$  mW per Hz receiver bandwidth, so a noise factor of  $\epsilon = 1$  in this analysis represents a very quiet detector system, especially when dealing with milliWatt optical powers.

The signal-to-noise ratio of equation (3) is plotted as a function of modulation depth in Fig. 6 for various different fringe visibilities, ranging from almost ideal ( $V = 0.9999$ ) to very non-ideal ( $V = 0.5$ ), assuming no measurable electronic noise ( $\epsilon = 0$ ). Similar plots are also obtained for different electronic noise levels  $\epsilon > 0$ . Clearly, the greater the unrelated shot noise due to the imperfect dark fringes, the more high-frequency modulation is required to optimise sensitivity. On each curve, the optimum signal-to-noise occurs when the modulation-induced shot noise becomes the dominant noise contribution. The general sensitivity roll-off at modulation depths beyond the optimum indicates that the extra modulation produces more noise than signal.

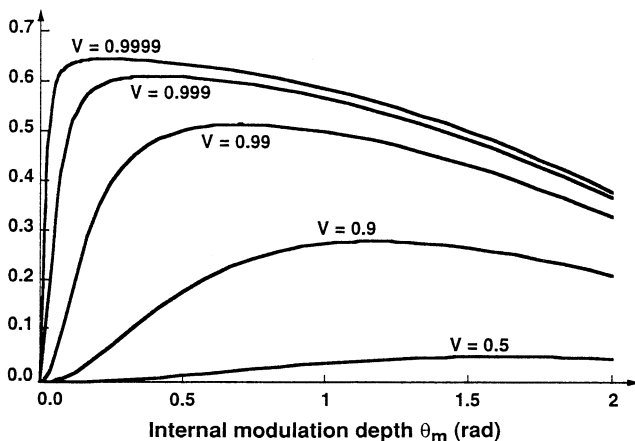


**Fig. 6.** Internal modulation signal-to-noise ratios plotted against internal modulation depth  $\theta_m$  from equation (3) for several non-ideal interferometers with imperfect fringe contrast but no detector noise ( $V < 1$  and  $\epsilon = 0$ ). These values have been normalised to the best achievable signal-to-shot-noise ratio in the direct detection system for the same input power and signal strength. In the ideal limit ( $V = 1$  and  $\epsilon = 0$ ) the normalised internal modulation signal-to-noise ratio approaches  $2/3$ . The greater the light leakage at the dark fringe, the greater the required  $\theta_m$  for optimal performance.

As  $V \rightarrow 1$  and  $\epsilon \rightarrow 0$ , the optimum modulation depth  $(\theta_m)_{\text{opt}}$  approaches zero. In this limiting condition, the signal-to-noise ratio in the internal modulation scheme approaches

$$(S/N)_{\text{max}} \rightarrow \frac{2}{3} \rho P_{\text{in}} \theta_s^2 / 4eB. \tag{5}$$

Here we assume very small signals, so that  $J_1(\theta_s) \rightarrow \theta_s/2$ . The shot-noise-limited sensitivity of an ideal internally-modulated interferometer is the phase signal  $(\theta_s)_{\text{min}}$  which produces a demodulated output with the same amplitude as the rms demodulated shot noise at the receiver:

$$(\theta_s)_{\text{min}} \rightarrow \sqrt{\frac{3}{2}} (4eB / \rho P_{\text{in}})^{1/2} \approx 1.225 (\theta_s)_{\text{direct}}. \tag{6}$$

This represents a 22.5% penalty compared to the best possible shot-noise-limited sensitivity  $(\theta_s)_{\text{direct}}$  achieved with direct detection using the same signal, bandwidth,

input power and detectors. Provided the interferometer fringe contrast is kept sufficiently high, and electronic noise is kept extremely low, it is possible to come arbitrarily close to the sensitivity in equation (6) in the internal modulation scheme.

The  $\sqrt{\frac{3}{2}}$  phase sensitivity penalty relative to the direct detection scheme is entirely a result of demodulating non-stationary shot noise associated with the 100% intensity modulation at the output of an ideal interferometer (Niebauer *et al.* 1991; Mio and Tsubono 1992; Gray *et al.* 1993). The only way to avoid this penalty is to use the information contained at higher frequencies in the noise spectrum. This requires the use of more sophisticated modulation and demodulation waveforms containing higher harmonics of the modulation frequency to exploit frequency correlations in the modulated noise spectrum, thereby reducing the demodulated noise towards the standard shot noise limit (Meers and Strain 1991; Gray *et al.* 1993).

Fig. 7 shows the optimum modulation depth  $(\theta_m)_{opt}$  as a function of electronic noise and interferometric fringe visibility in non-ideal systems. When the interferometer and detectors are nearly perfect, very weak modulation is required. However, even extremely small levels of electronic noise or dark fringe transmission necessitate large internal modulation depths to optimise the sensitivity.

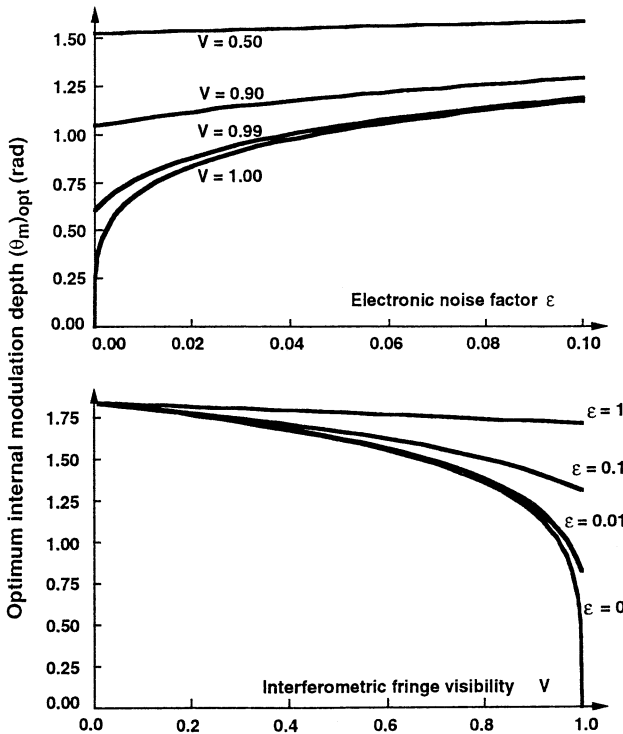
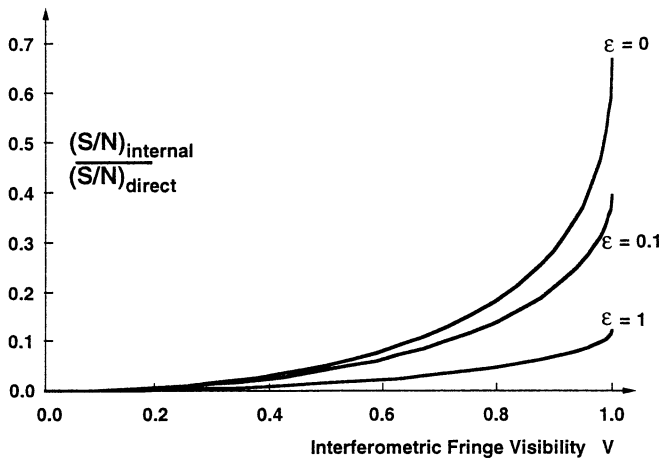


Fig. 7. Internal modulation depth  $\theta_m$  required to optimise the signal-to-noise ratio in the internal modulation scheme, plotted against fringe visibility  $V$  and electronic noise factor  $\epsilon$ , when the interferometer is non-ideal. Very small levels of unrelated background noise necessitate strong modulation depths.

Finally, in Fig. 8, we plot the best-case signal-to-noise ratio in the internal modulation scheme (normalised to the ideal direct detection limit) as a function of interferometric fringe visibility  $V$ , for different levels of electronic noise  $\epsilon$ , assuming that the optimum modulation depth  $(\theta_m)_{\text{opt}}$  is used, and assuming that the average Michelson mirror reflectivity  $R$  is as large as possible for the given value of  $V$ . [In our analysis  $V < 1$  only if the two mirrors differ; mode matching is considered perfect here. Modal imperfections leading to imperfect fringes can be readily modelled by equivalent mirror losses for most purposes. In this picture, the range of possible  $V$  values is constrained by  $R$ : for  $R < 0.5$ , all  $V$  values from 0 to 1 are physically allowed, while for  $R > 0.5$ ,  $V$  must lie between  $\sqrt{(2R-1)}/R$  and 1. Likewise, for any  $V$ , there is a maximum possible value of  $R$ . This maximum value of  $R$  is assumed here because it sets an upper limit on the signal-to-noise ratio for a given  $V$ .]

Imperfect fringes or measurable amounts of electronic noise severely reduce the overall interferometric sensitivity in this scheme, even if the optimum modulation depth is used. The ideal ( $\epsilon = 0$ ) curve in Fig. 8 approaches a normalised signal-to-noise ratio of  $\frac{2}{3}$  at  $V = 1$ . The attainable sensitivity in the internal modulation scheme is reduced by a factor of 2 when the dark fringe transmission represents just under 4% of the input light (or when electronic noise corresponds to the shot noise which this leakage would produce at the detector). In this condition, Fig. 7 shows that an internal modulation amplitude of  $\sim 1$  rad is required to maximise sensitivity.



**Fig. 8.** Maximum possible signal-to-noise ratio obtainable in the internal modulation scheme, as a function of fringe visibility  $V$ , for various different electronic noise levels. The optimum modulation depth  $\theta_m$  as plotted in Fig. 7 has been assumed, and again the S/N is normalised to the best achievable direct detection S/N value for the same signal and input power.

### (2e) Signal and Noise Demodulation in the External Modulation Scheme

The signal and noise analysis of the external modulation system is reasonably involved (Man *et al.* 1990; Gray *et al.* 1995), and we shall not describe it in great detail here, apart from pointing out key features for comparison to the internal modulation scheme. The external modulation configuration of Fig. 3 exploits

waveform asymmetry to extract signal information in much the same way as the internal scheme, to the extent that the output waveforms at each detector can, in some instances, appear very similar to those obtained by internal modulation (see Fig. 4*b*) with the exception of a significant DC offset due to the average power seen at the detectors. This average power is due mostly to the local oscillator, since the Michelson is tuned closely to a dark fringe and contributes little light in the optimal configuration.

The high-frequency modulation in the local oscillator arm serves to rapidly re-arrange a small fraction of this total power between the two detectors, much as in any Mach-Zehnder interferometer. If the DC phase of the local oscillator beam is set so that each detector receives equal power in the absence of any signal phase in the Michelson interferometer, the waveform asymmetries induced by low-frequency signals in the Michelson are equal and opposite in each detector. It proves beneficial, therefore, to detect both beam combiner outputs and to subtract one from the other—this eliminates much of the common mode noise and more importantly doubles the amplitude of the frequency-shifted signals entering the mixer. The mixer output in these cases can exactly resemble that produced by the internal modulation system (see Fig. 5), depending on the amount of dark fringe transmission by the Michelson.

The shot noise, which is uncorrelated at each detector, is only increased by a factor of  $\sqrt{2}$  by the subtraction process, and hence detecting and subtracting the two beam combiner outputs improves the signal-to-noise ratio by a factor of  $\sqrt{2}$  compared to detecting only one output.

The important controllable parameters in the external modulation scheme are the external modulation depth  $\theta_m$  (rad), and the optical power fraction  $\alpha$  transmitted to the interferometer. The remaining fraction  $1-\alpha$  is tapped off into the local oscillator beam.

Here, as with the internal modulation scheme, the demodulated signal is proportional to  $J_1(\theta_m)$ . However, in this scheme, the demodulated shot noise is independent of  $\theta_m$  since the *total* optical power detected by the two detectors does not vary with the phase of the Mach-Zehnder interferometer. Hence, the optimum modulation depth is simply that which maximises  $J_1(\theta_m)$ , namely  $\theta_m = 1.84$  rad. The fact that shot noise does not depend on  $\theta_m$  also eliminates the non-stationary shot noise effects which penalise the signal-to-noise ratio in the internal modulation scheme.

In the external modulation scheme, the optimal optical power fraction  $\alpha$  transmitted to the interferometer is subject to a tradeoff similar to that which determined the optimum value of the modulation depth  $\theta_m$  in the internal modulation scheme. Here, the frequency-shifted signal strength at  $\omega_m \pm \omega_s$  is proportional to the product of the electric field amplitudes interfering at the detector from the Michelson and local oscillator beams, which are in turn proportional to  $\sqrt{\alpha}$  and  $\sqrt{1-\alpha}$  respectively. Hence the demodulated signal strength at the mixer output should vary as  $\sqrt{[\alpha(1-\alpha)]}$ .

The demodulated noise varies in proportion to  $(1-\alpha) + \alpha(R/2)[1 - VJ_0(\theta_s)] + 2\epsilon$ , due to shot noise contributions from the local oscillator and Michelson interferometer and also electronic noise.

After some careful analysis (Gray *et al.* 1995), the demodulated signal-to-noise *power* ratio, measured at a receiver at the mixer output, can be shown to be

$$S/N = \frac{(4\rho P_{in}/eB)R(1+V)\alpha(1-\alpha)J_1^2(\theta_s/2)J_1^2(\theta_m)}{1-\alpha + \alpha(R/2)[1-VJ_0(\theta_s)] + 2\epsilon}, \tag{7}$$

where  $\rho$ ,  $P_{in}$ ,  $B$ ,  $e$ ,  $R$ ,  $V$ ,  $\theta_s$  and  $\theta_m$  are exactly as previously defined below equation (3),  $\alpha$  is the power fraction of the input light which is transmitted to the Michelson ( $0 \leq \alpha \leq 1$ ), and  $\epsilon$  is once again a normalised electronic noise factor, calculated based on the performance of each detector just as it was in the internal modulation scheme. Again, the use of optimal optical phases and demodulation quadratures has been assumed in deriving (7).

Increasing the optical power in the local oscillator arm (decreasing  $\alpha$ ) leads initially to larger demodulated signals and larger shot noise. This happens at the expense of light passing to the Michelson. Optimum signal-to-noise will occur when the optical tap-off fraction has increased to the point where the shot noise contribution from the local oscillator just dominates the overall noise. Greater tap-off ratios yield no further signal-to-noise improvement, since the dominant  $1-\alpha$  factor in the denominator would cancel the  $1-\alpha$  in the numerator, and the signal-to-noise would decrease with  $\alpha$ .

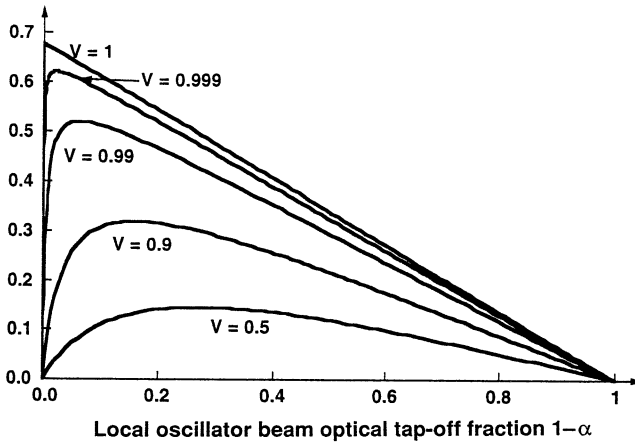


**Fig. 9.** External modulation signal-to-noise ratios, plotted against the optical tap-off fraction  $1-\alpha$  from equation (7), for several non-ideal interferometers with imperfect fringe contrast but no detector noise ( $V < 1$  and  $\epsilon = 0$ ). This normalised plot is very similar to Fig. 6. In the ideal limit ( $V = 1$  and  $\epsilon = 0$ ) the normalised external modulation signal-to-noise ratio approaches  $0.676$ . The greater the light leakage at the dark fringe, the greater the required optical tap off fraction  $1-\alpha$  for optimal performance.

Fig. 9 plots the demodulated signal-to-noise ratio in the external modulation scheme as a function of the optical power tap-off fraction  $1-\alpha$ , assuming perfectly quiet detectors and various interferometric fringe visibilities  $V$  in the Michelson interferometer. Evidently greater levels of unrelated noise (shot noise in this case due to light leakage from the Michelson at lower values of  $V$ ) necessitate greater tap-off ratios  $1-\alpha$  to optimise the signal-to-noise, and lead to lower achievable signal-to-noise ratios. Increasing levels of electronic noise have a similar effect. This plot resembles Fig. 6 in many ways.

Fig. 10a plots the optimum value of the tap-off ratio as a function of unrelated electronic noise, while Fig. 10b shows the optimum optical tap-off ratio as a

function of interferometric fringe visibility. The required tap-off increases very rapidly for small unrelated noise factors, just as the optimum value of internal modulation depth  $\theta_m$  did in Fig. 7 above. Any practical system will require a measurable amount of light in the local oscillator arm, in general.

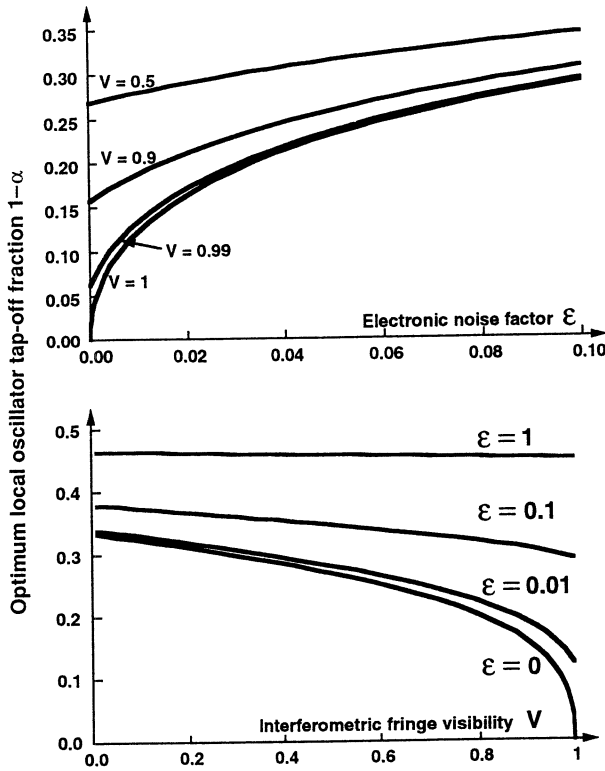


**Fig. 10.** Optical tap-off fraction depth  $1-\alpha$  required to optimise the signal-to-noise ratio in the external modulation scheme, plotted against fringe visibility  $V$  and electronic noise factor  $\epsilon$ , when the interferometer is non-ideal. Very small levels of unrelated background noise necessitate large levels of light in the local oscillator beam.

Fig. 11 plots the resulting demodulated signal to noise seen at the output of an external modulation system as a function of the fringe visibility  $V$  of the Michelson interferometer, assuming that optimum tap-off fractions, modulation depths, optical phases etc. are used, and again assuming the largest value of  $R$  for each  $V$ , to give an upper limit on the achievable signal-to-noise. This is very reminiscent of the best case plots obtained for internal modulation, except that here, the signal-to-noise drops off more slowly with  $V$  for imperfect interferometers, and does not rise quite as high for  $V = 1$ .

In the limiting case of a perfect interferometer ( $R = 1$  and  $V = 1$ ) and no electronic noise ( $\epsilon = 0$ ), it can be shown that the signal to noise approaches a value almost identical to that which applies to the internal modulation scheme:

$$(S/N)_{\max} \rightarrow 0.676(\rho P_{\text{in}} \theta_s^2 / 4eB). \tag{8}$$

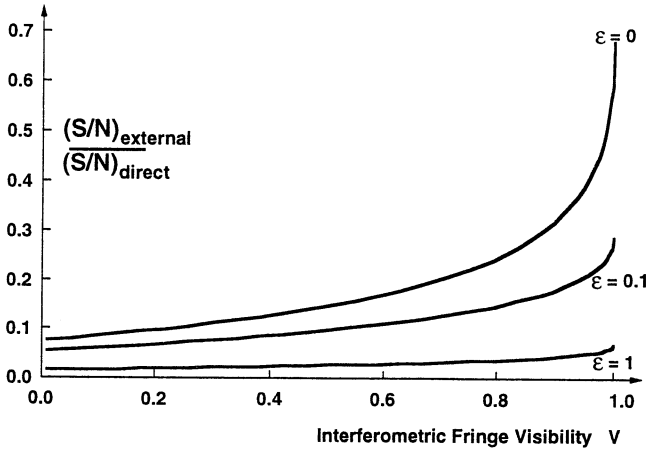


**Fig. 11.** Maximum possible signal-to-noise ratio obtainable in the external modulation scheme, as a function of fringe visibility  $V$ , for various different electronic noise levels. The optimum tap-off ratio  $1-\alpha$  as plotted in Fig. 10 has been assumed, and again the S/N is normalised to the best achievable direct detection S/N value.

The resulting sensitivity limit is given by

$$(\theta_s)_{\min} \rightarrow \sqrt{0.676(4eB/\rho P_{\text{in}})^{\frac{1}{2}}} \approx 1.216(\theta_s)_{\text{direct}}. \quad (9)$$

The 21.6% sensitivity penalty relative to the direct detection scheme is due to inefficiencies inherent in the simple signal recovery process modelled here, i.e. the use of simple sinusoidal modulation and demodulation waveforms. The strong modulation in the local oscillator arms produces large sidebands at many higher harmonics of the modulation frequency, but only the fundamental harmonics are demodulated; the remaining modulation sidebands represent wasted optical power. In principle, it is possible to approach the direct detection sensitivity  $(\theta_s)_{\text{direct}}$  by the use of more sophisticated modulation and demodulation waveforms (involving higher harmonics) to create and exploit frequency correlations in the signal spectrum, and thereby improve the demodulated signal towards the level obtained by direct detection.

The similarity between the inherent limiting sensitivities experienced in the internal and external modulation scheme is largely coincidental—the mechanisms leading to these two penalties are only distantly related. Both penalties can be ascribed mathematically to non-optimal modulation and demodulation strategies (for signal in the external modulation scheme, and shot noise in the internal modulation scheme). Even in non-ideal cases ( $\epsilon > 0$  and  $V < 1$ ), the internal and external modulation schemes possess very similar sensitivities in general. In practice, this means that the choice of modulation scheme depends entirely on practical and experimental considerations.

### 3. Experimental Demonstration of Shot-noise-limited Phase Measurements using Phase Modulation Interferometry

Our analysis in the previous section of non-ideal modulated interferometers only accounts for a few physical features of a practical interferometric system, for simplicity, but even a simple generic model has little application until it can be experimentally verified in controlled conditions. Here we describe briefly some laboratory benchtop-scale experiments performed to investigate both the internal and external modulation schemes, to compare the achievable sensitivity with the theoretical predictions, and to assess key experimental issues which affect the usefulness of each scheme. Sections 3a and 3b below summarise experiments performed using a polarimetric electric field sensor to investigate the internal modulation scheme. These experiments and theoretical background are described in detail in Stevenson *et al.* (1993). Section 3c is a summary of experiments performed using a Michelson interferometer to investigate the external modulation technique. A full description of these experiments and theory can be found in Gray *et al.* (1995).

#### (3a) Direct Detection Experiments using a Reflective Polarimetric Sensor

A polarimeter is topologically identical to other simple two-beam interferometers in that it splits light into two independent beams (orthogonal polarisation states). These propagate independently through a medium which imposes a differential phase signal (an electro-optic crystal whose birefringence changes in response to external electric fields, thus altering the retardance or optical path difference for the two orthogonal polarisation states) and the two beams are recombined at a beam combiner (polarising beamsplitter/combiner) which allows them to interfere to produce complete interference fringes. A polarimeter has an advantage over other two-beam interferometers—both beams traverse the same optical path to and from the birefringent medium, so most phase disturbances and drifts are ‘common mode’ and have no effect on the output intensity. In particular, very stable, high quality dark fringes are possible without active locking techniques, since birefringence variations across the optical wavefronts only arise within optical components, and are generally extremely small and constant in time.

Our sensor was configured as a reflective polarimeter, using the same polarising cube to split the light into its orthogonally polarised components and to recombine them on return from a mirrored sensing crystal. Initially we used this device in a direct detection configuration, to investigate its viability as a non-invasive sensor scanning high-frequency oscillating electric field distributions in the vicinity of test circuit patterns. These trials proved very successful at signal frequencies above 12 MHz, where the detected light was shot noise limited. The visibility  $V$  of the interferometer was measured to be around 0.9998, and with 18 mW of input light at 1064 nm, the detector and amplifiers were quiet enough to achieve an effective electronic noise factor  $\epsilon$  of just 0.0066.

Despite the low level of unrelated noise, it was still necessary to detune the polarimeter significantly from a dark fringe to allow the signal to be measured. The optimum signal-to-noise ratio was observed when the polarimeter was tuned 0.37 rad away from its dark fringe, and the resulting phase sensitivity was 0.25  $\mu$ rad in a resolution bandwidth of 1 kHz at the receiver, very close to the

theoretically predicted  $0.26 \mu\text{rad}$ . The corresponding measured spectral phase sensitivity was  $8 \times 10^{-9} \text{ rad Hz}^{-\frac{1}{2}}$ , only 11% above the ideal limit for a noiseless interferometer operating at a dark fringe. The polarimeter was also found to be less sensitive with less input light, exactly in accordance with the theory that the signal strength varies in proportion to the optical power while shot noise scales as the square root of the optical power.

### (3b) Internal Modulation Experiments

Having verified the simple analytic model for direct detection in the non-ideal interferometer, we measured the sensitivity achievable using internal modulation for signals below 12 MHz, where laser technical noise dominated. The light source was a Nd:YAG MISER very similar to the one whose intensity noise spectrum is plotted in Fig. 1a; in particular, our MISER exhibited a large relaxation oscillation at around 0.5 MHz. Internal retardance modulation at 25 MHz was produced by means of an electro-optic crystal inserted in the beam path between the polarising cube and the reflective sensing crystal.

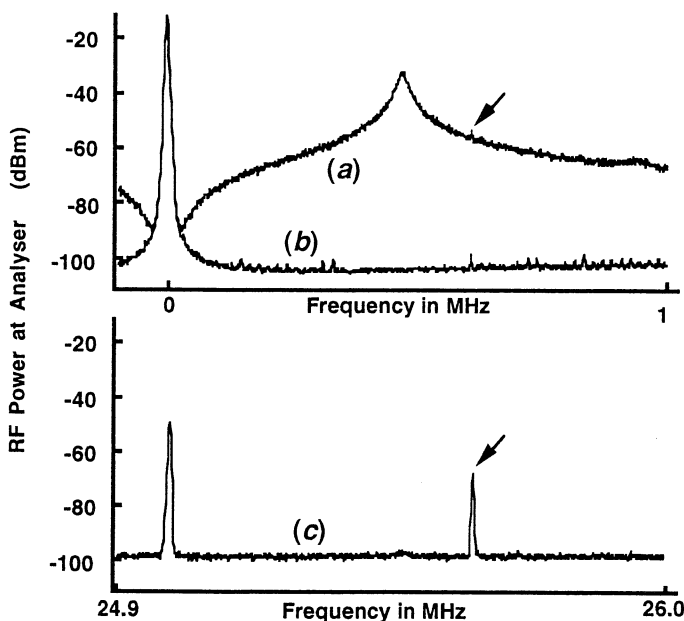


**Fig. 12.** Results of the internal modulation trials using a reflective polarimeter sensing a signal at 621 kHz, well within the technical noise band of the laser source. (a) Signal and noise power spectra obtained using the direct detection method—the signal is just visible (arrow) above the wings of the relaxation oscillation peak of the laser. (b) Electronic noise floor of the detector and receiver system in the direct detection configuration. (c) Frequency-shifted signal and noise floor in the internal modulation configuration, showing  $\sim 70$  dB suppression of the technical noise spectrum, and a net improvement of more than 30 dB in the signal-to-noise ratio. The system is still limited by electronic noise in this case.

Low-frequency signals were again induced in the reflective sensing crystal, and at 621 kHz, the signal was deliberately applied in a region of large technical noise on the wings of the relaxation oscillation peak. The signal amplitude was

made large enough so that we were just able to resolve, on a spectrum analyser, the signal peak above the technical noise floor of the laser using the direct detection system. Fig. 12a shows the resulting signal and noise spectra obtained using the direct detection method. The chief feature on this noise floor is the giant relaxation oscillation peak. Clearly, signals at this particular frequency comparable to the shot noise using this resolution bandwidth would be obscured by optical noise many orders of magnitude larger.

When internal phase modulation was imposed and the interferometer was tuned to a dark fringe at its output, Fig. 12b shows how the same signal now appeared 33 dB above the electronic noise floor in the frequency-shifted spectrum. Technical noise was suppressed by about 7 orders of magnitude (the relaxation peak was barely discernable in the frequency-shifted power spectrum) confirming how well the dark fringe is passively maintained in a polarimeter. Experimentally, we found that optical phase displacements of just a few milliradians re-introduced high levels of technical noise into the output power spectrum. Clearly, large signal-to-noise improvements are possible using internal modulation in frequency ranges dominated by light source noise, provided very strict dark fringe stability is maintained.

Interestingly, despite the massive suppression of technical noise and excellent dark fringe stability of our polarimeter, we were not able to achieve true shot-noise-limited sensitivity in our internal modulation trials. The principle problem here was electronic noise in the detection system. Fig. 6 above shows that as the unrelated noise increases, greater modulation depth is required to optimise the signal-to-noise ratio. For an electronic noise factor  $\epsilon = 0.0066$ , the signal-to-noise ratio varies with modulation depth in a manner similar to that plotted in Fig. 6 for  $V = 0.99$ . Surprisingly perhaps, to make the measurement shot-noise-limited and optimise the sensitivity with this low level of electronic noise, we would need around 0.7 rad of modulation amplitude, far larger than the 0.11 rad we were able to achieve with our available electro-optic modulator and associated driving electronics. Alternatively, we could have made a shot-noise-limited measurement with this particular modulator, if the input power had been 60 times larger (1.1 W) or if the electronic noise had been reduced by a factor of 60 ( $\epsilon = 1.1 \times 10^{-4}$ ).

With a modulation depth of 0.11 rad, the measured signal-to-noise ratio only reached 15% of its ideal maximum value, compared to a theoretical prediction of 18%, a reasonable agreement with the analysis given the experimental errors involved in this type of measurement. The minimum resolvable phase retardance turned out to be  $0.85 \mu\text{rad}$  in a 1 kHz bandwidth, corresponding to a spectral phase sensitivity of  $2.6 \times 10^{-8} \text{ rad Hz}^{-\frac{1}{2}}$ , about 2.6 times larger than the ideal theoretical limit of  $1.0 \times 10^{-8} \text{ rad Hz}^{-\frac{1}{2}}$  for this input light level.

### (3c) External Modulation Experiments

We constructed a Michelson interferometer and tapped a local oscillator off the input beam in much the same way as shown in Fig. 3. The light source was again a Nd:YAG MISER, emitting at 1064 nm and with a strong relaxation oscillation peak in the noise spectrum at around 300 kHz. A low-frequency phase signal at 2 MHz was introduced into one arm of the Michelson using a phase modulator. The Michelson had arm lengths of around 0.15 m, and was tuned to a dark fringe. The attenuation due to the modulator was compensated by a

neutral density filter in the second arm, and the geometric foreshortening of the diverging beam inside the high-index modulator was offset by placing the other mirror slightly closer to the beamsplitter. This geometric modematching measure actually increases the mismatch between the two-way optical propagation times in each arm, in this case, equivalent to a length mismatch of around 60 mm experimentally. This in turn is capable of converting laser frequency noise into unwanted intensity noise at the output, but this effect proved to be negligible over most frequencies of interest here.

Maximum interferometric fringe visibilities  $V$  of up to 0.9967 were attained (corresponding to fringe contrast ratios of about 600:1), but this could only be maintained by active servo locking. To lock the interferometer to its dark fringe, with minimal rms phase excursions, the 75 MHz component in the output of the signal subtractor (see Fig. 3) must be nulled. This was monitored by looking at the DC output of the mixer. The resulting 'error signal' was integrated, filtered and fed to a piezo-electric mirror mount at the end of one arm of the Michelson. This locked the interferometer to its dark fringe automatically, cancelling out drifts, vibrations and acoustic noise out to about 5 kHz, provided the local oscillator was set to within about  $45^\circ$  of its correct optical phase. The local oscillator phase was adjusted manually in this experiment, which proved satisfactory most of the time. The bright fringe from the Michelson was directed towards the laser, so an optical isolator in front of the laser and a small amount of mirror misalignment was required to prevent optical feedback effects.

A resonant tuned phase modulator in the local oscillator beam provided the high-frequency phase modulation, in this case at 75 MHz. The Michelson output beam and local oscillator were combined at a 50:50 beamsplitter cube, and the outputs focussed onto a pair of balanced InGaAs detectors. The Mach-Zehnder interferometer exhibited an effective fringe contrast of about 150:1 when equal power was arranged in the local oscillator and Michelson output arms, more than adequate for optimal operation of this experiment.

In this experiment, the input power was measured to be 9 mW, and  $\epsilon = 0.04$ . The electronic noise dominated the background noise dictating the optimum optical tap-off fraction  $1-\alpha$  for the local oscillator beam. The dark fringe transmission of our interferometer would need to be around 60 times brighter ( $V \sim 0.9$ ) for the extra shot noise to be comparable to the measured electronic noise. Fig. 9 shows how increasing background noise requires larger optical tap-off ratios to optimise sensitivity. For  $\epsilon = 0.04$ , the signal-to-noise ratio varies with the tap-off fraction in a manner very similar to the curve plotted in Fig. 9 for  $V = 0.9$ . The tap-off fraction was adjusted to its optimum value (roughly 20% in this experiment) by means of optical waveplates and a polarising beamsplitter.

Shot-noise-limited performance was achieved in this external modulation experiment. From the analysis described in Section 2, we could predict how sensitivity would vary with the modulation depth imposed in the external beam arm. As it happened, we were only able to impose a maximum of 1.18 rad of modulation in the local oscillator arm, well short of the 1.84 rad required for optimum performance, as the inductive core inside the resonant modulator saturated above a particular driving voltage.

Phase sensitivity was inferred by adjusting the signal strength in the Michelson to produce a demodulated signal-to-noise ratio of 1 at the receiver for each

different modulation depth used. Fig. 13 shows how the predicted and measured spectral phase and displacement sensitivity varied with the applied modulation depth  $\theta_m$  in the local oscillator beam. Clearly, there is excellent agreement with the theoretical predictions, indicating that the simple analysis is useful in predicting performance in this kind of system. A similar test using a constant strong signal in the Michelson (producing a signal-to-noise ratio in the vicinity of 20 to 40 dB), and variable modulation in the external arm, also showed exact agreement with theory.

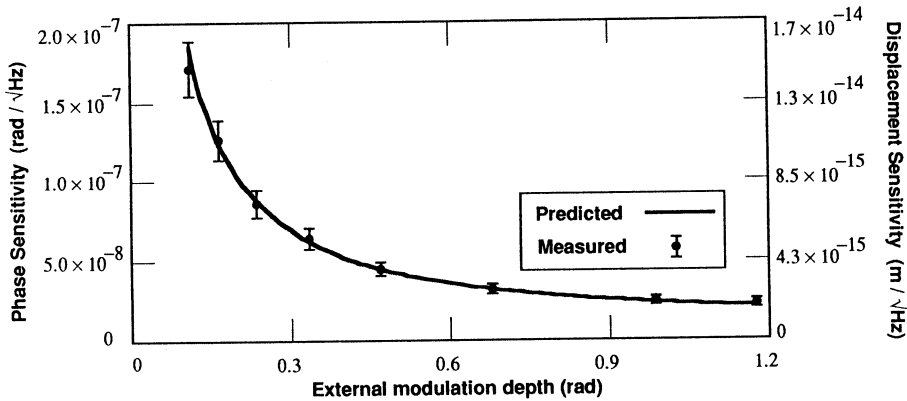


Fig. 13. Predicted and measured phase and displacement sensitivities in the external modulation scheme, plotted against the external modulation depth  $\theta_m$ , obtained with a signal at 2 MHz. This system successfully produced shot-noise-limited performance in a region of the spectrum dominated by technical noise using direct detection.

The best shot-noise-limited phase sensitivity achieved experimentally using this system was  $2.0 \times 10^{-8}$  rad  $\text{Hz}^{-\frac{1}{2}}$ , corresponding to a displacement sensitivity of  $1.7 \times 10^{-15}$  m  $\text{Hz}^{-\frac{1}{2}}$ , imposing a modulation depth of 1.18 rad on the external beam. The sub-optimal external modulation depth cost us about 15% in sensitivity for this electronic noise level. For the same input power, assuming optimum external modulation depth, a perfect interferometer and noiseless detection system, the predicted ideal sensitivity would have been  $1.2 \times 10^{-8}$  rad  $\text{Hz}^{-\frac{1}{2}}$ , so our system suffered a 66% sensitivity penalty relative to the ideal limit.

The shot-noise-limited performance for signals at 2 MHz was repeatable until the signal frequency dropped to around 100 kHz, below which laser frequency noise effects dominated the shot noise floor. A series of peaks appeared in the output power spectrum, harmonics of a fundamental component at about 30 kHz, and were found to be associated with a laser frequency noise with an estimated spectral density of 3 mrad  $\text{Hz}^{-\frac{1}{2}}$  at 30 kHz, coupled into the intensity noise spectrum by the 60 mm arm length mismatch.

### (3d) Key Points raised by the Modulated Interferometer Experiments

Our internal and external modulation experiments raised some key points of general interest to anyone contemplating using these schemes in a practical sensor:

(i) Direct detection interferometry provides the best sensitivity in general, but only when the signal is at a sufficiently high-frequency that laser technical noise is dominated by shot noise at the detector.

(ii) Good dark fringe stability is essential in suppressing technical noise to below the shot noise level. If this cannot be achieved passively, active servo locking to the dark fringe condition should be arranged. An rms optical phase stability of around 1 mrad is sufficient to suppress technical noise many orders of magnitude greater than shot noise. The bandwidth of the servo system should be chosen to handle the likely spectrum of mechanical disturbances to the Michelson interferometer.

(iii) The phase sensitivity of the external modulation system is best when the optical phase of the local oscillator beam is adjusted to produce equal outputs on the two detectors (when the Michelson is set to a dark fringe). The sensitivity only depends weakly on the local oscillator phase near this condition, so the locking requirements are more relaxed than for the Michelson interferometer phase.

(iv) Unrelated electronic and dark fringe shot noise in the system must be kept to an absolute minimum in both modulation schemes. In general, one of these contributions will tend to dominate the other, and most effort should therefore be put into reducing the dominant noise source. It is desirable to reduce the unwanted light leakage to less than about 1% of the input light level, so that the achievable signal-to-noise is within about 1 dB ( $\sim 20\%$ ) of the ideal limit. Similarly, electronic noise should be less than about 1% of the shot noise which would be measured if all of the input light was detected on a single detector.

(v) To optimise the signal-to-noise ratio in the internal modulation scheme when unrelated noise is present in the system, a modulator capable of imposing a strong internal phase modulation must be available. When unrelated noise is kept below the 1% level nominated in (ii), a modulation depth of 1 rad should be sufficient to optimise the sensitivity of the instrument.

(vi) A modulator capable of producing 1.84 rad of modulation is required in the external modulation scheme to optimise sensitivity.

(vii) Significant optical tap-off ratios are usually required in the external modulation system when unrelated background noise exists in the system. This requires detectors each capable of safely handling up to say 10% of the maximum input light without saturation or destruction, otherwise the detectors may limit the input power which can be used. There also needs to be a suitable adjustable beamsplitting arrangement to optimise the tap-off ratio.

(viii) Optical path lengths in each arm of the Michelson interferometer need to be well matched to avoid the conversion of laser frequency noise into laser intensity noise. The degree of length matching required depends on the amount of frequency noise in the laser in the signal frequency range of interest.

(ix) RF phase delays between detectors and mixers have to be chosen carefully to match those between the high-frequency signal generator and the mixer, to allow proper demodulation of the signal. The higher the modulation frequency, the more critical is the RF path matching requirement. An adjustable RF phase delay is desirable here.

#### 4. General Considerations in selecting an Optical Modulation Scheme

So far in this paper, we have described the operation and implementation of two interferometric modulation schemes. Because both schemes have similar inherent sensitivities, the choice of which modulation scheme is best to use will

usually depend on practical factors, peculiar to each application. Here we briefly discuss two possible considerations affecting this choice.

#### *(4a) Complexity of Implementation*

The external modulation scheme is fundamentally more complex than the internal modulation scheme. Three electric fields interfere at each of the two detectors in the external modulation configuration, one field from each beam arm of the Michelson interferometer and one from the local oscillator beam. This complicates both the analysis and practical implementation of the external modulation scheme relative to the internal modulation scheme as it is necessary to control independently and perhaps servo-lock two DC optical phases in this system: the differential phase in the Michelson interferometer, and the DC phase of the local oscillator beam relative to the absolute output phase of the light from the Michelson at the detectors. The two phase-locking servos will also interact, and the overall stability is not simple to predict.

It is also necessary to optimise the fraction of optical power tapped off into the local oscillator beam (the Michelson interferometer still requires equal amplitude beams for proper dark fringe interference) and, of course, the high-frequency phase modulation depth in the local oscillator. This very complexity may be sufficient for many users to opt for the simpler internal modulation scheme.

#### *(4b) Beam Distortion Effects*

Interferometric gravitational wave detectors will not be using internal modulation for the simple reason that the presence of optical modulators in the Michelson arms distorts and partially absorbs the beams. The presence of phase modulators in the beam arms can have several deleterious effects:

(i) Optical contrast is severely reduced by wavefront distortions. As a result there is unwanted optical power at the output and unwanted shot noise.

(ii) Pockels cells have several percent loss. This will limit the build up of light in optical recycling systems and reduce the achievable sensitivity gain.

(iii) Large scale gravitational wave interferometers will have large diameter beams or very high optical power. It is difficult to find high-frequency phase modulators of sufficient optical quality and linearity of response for such applications.

It was to avoid these practical drawbacks in large scale high-power gravity wave interferometers that the external modulation method was proposed in the first place.

## **5. Conclusions**

We have demonstrated analytically and experimentally that phase modulation interferometry is a powerful method for extracting low-frequency phase signals with shot-noise-limited sensitivity, when the same phase variations would be obscured by technical noise of a light source many orders of magnitude greater using direct detection techniques.

We have described two particular techniques of phase modulation interferometry in this article: internal modulation and external modulation. In both schemes, high-frequency phase modulation shifts low-frequency signals into a shot-noise-limited region of the photocurrent spectrum, and subsequent mixing with the modulation waveform recovers the low-frequency signal information, free of technical noise

from the light source provided the sensing interferometer is set to produce a dark fringe at its output. Internal modulation imposes its modulation within the sensing interferometer, while external modulation imposes phase modulation on a local oscillator beam which is subsequently recombined with the output of the sensing interferometer.

We used a simple analytic model to predict the sensitivity of both modulation schemes in the presence of non-ideal features—electronic noise in detectors and amplifiers, and unwanted optical transmission at the dark fringe of the interferometer. In both schemes, as the electronic noise and dark fringe transmission is reduced, the shot-noise-limited sensitivity is predicted to approach about 67% of the maximum shot-noise-limited signal-to-noise ratio achievable using direct detection in an ideal noiseless interferometer. This penalty is due to the fact that simple sinusoidal modulation and demodulation is inefficient as it loses signal or noise information to higher harmonics in the spectrum. We found that, even in non-ideal cases, the two interferometric modulation schemes have comparable sensitivity, so that the choice of which scheme to use in a given situation depends largely on practical and experimental considerations.

Experimentally we used these phase modulation interferometry techniques to suppress technical noise power in the photocurrent spectrum by up to 7 orders of magnitude in an internally modulated polarimeter, and to retrieve signals at frequencies as low as 100 kHz with shot-noise-limited sensitivity using an externally modulated Michelson interferometer. Using only 9 mW of input light in the external modulation configuration, we achieved a spectral phase sensitivity of just  $2.0 \times 10^{-8}$  rad Hz $^{-\frac{1}{2}}$ , comparable to the shot-noise-limited sensitivity predicted analytically for an ideal externally modulated interferometer. Comparable sensitivity was achieved in the internal modulation scheme, and found to be consistent with the predictions of the simple analysis described earlier. These two modulation techniques should be applicable to a wide variety of interferometric sensors which require shot-noise-limited sensitivity.

## References

- Bachor, H.-A., and Fisk, P. T. H. (1989). *Appl. Phys. B* **49**, 291.  
 Bachor, H.-A., and Manson, P. J. (1990). *J. Mod. Opt.* **37**, 1727.  
 Born, M., and Wolf, E. (1980). In 'Principles of Optics', 6th edn (Pergamon: Oxford).  
 Brillet, A., Jacquemet, M., Giazotto A., *et al.* (1992). 'VIRGO Final Conceptual Design' (LAL: Orsay).  
 Caves, C. M. (1980). *Phys. Rev. Lett.* **45**, 75.  
 Caves, C. M. (1981). *Phys. Rev. D* **23**, 1693.  
 Drever, R. P. W. (1983). Proc. Advanced Physics Institute on Gravitational Radiation, Les Houches, France (Eds N. Deruelle and T. Piran), p. 321 (North Holland: Amsterdam).  
 Fritschel, P. K. (1991). Techniques for laser interferometer gravitational wave detectors. PhD Thesis, MIT, Massachusetts.  
 Fritschel, P., Shoemaker, D., and Weiss, R. (1992). *Appl. Opt.* **31**, 1412.  
 Gea-Banacloche, J., and Leuchs, G. (1986). *J. Mod. Opt.* **34**, 793.  
 Gea-Banacloche, J., and Leuchs, G. (1987). *J. Opt. Soc. Am. B* **4**, 1667.  
 Gray, M. B., Stevenson, A. J., Bachor, H.-A., and McClelland, D. E. (1993). *Opt. Lett.* **18**, 759.  
 Gray, M. B., Stevenson, A. J., Harb, C. C., Bachor, H.-A., McClelland, D. E. (1995). *Appl. Optics* (to be published).  
 Harb, C. C. (1991). Stabilisation of a ring dye laser, MSc Thesis, ANU Dept. of Physics and Theoretical Physics.

- Harb, C. C., Gray, M. B., Bachor, H.-A., Schilling, R., Rottengatter, P., Freitag, I., and Welling, H. (1994). *IEEE J. Quant. Electron.* **30**, 2907.
- Heinrich, H. K., Bloom, D. M., and Hemenway, B. R. (1986). *Appl. Phys. Lett.* **48**, 1066.
- Hello, P. (1990). 'External Phase Modulation: upper limit for SNR', VIRGO internal report, Ref: 0.2.1.a (LAL: Orsay).
- Hough, J., *et al.* (1989). Proposal for a joint German-British interferometric gravitational wave detector. Max Planck Institut für Quantenoptik Report No. 147 (unpublished).
- Hough, J., *et al.* (1991). In 'The Detection of Gravitational Waves' (Ed. D. G. Blair), p. 329 (Cambridge University Press).
- Kane, T. J. (1990). *IEEE Phot. Tech. Lett.* **2**, 244.
- Loudon, R. (1981). *Phys. Rev. Lett.* **47**, 815.
- Man, C. N., Shoemaker, D., Pham Tu, M., and Dewey, D. (1990). *Phys. Lett. A* **148**, 8.
- Meers, B. J. (1988). *Phys. Rev. D* **38**, 2317.
- Meers, B. J., and Strain, K. A. (1991). *Phys. Rev. A* **44**, 4693.
- Michelson, A. A., and Morley, E. W. (1887). *Am. J. Sci.* (3rd Series) **34**, 333.
- Mio, N., and Tsubono, K. (1992). *Phys. Lett. A* **164**, 255.
- Niebauer, T. M., Schilling, R., Danzmann, K., Rüdiger, A., and Winkler, W. (1991). *Phys. Rev. A* **43**, 5022.
- Robertson, N. A., Hoggan, S., Mangan, J. B., and Hough, J. (1986). *Appl. Phys. B* **39**, 149.
- Rowan, S., Campbell, A. M., Skeldon, K., and Hough, J. (1994). *J. Mod. Opt.* **41**, 1263.
- Sandeman, R. J., and McClelland, D. E. (1990). *J. Mod. Opt.* **37**, 1747.
- Sasaki, O., and Okazaki, H. (1986). *Appl. Opt.* **25**, 3137.
- Stevenson, A. J., Gray, M. B., Bachor, H.-A., and McClelland, D. E. (1993). *Appl. Opt.* **32**, 3481.
- Strain, K. A. (1991). Techniques in laser interferometry for the detection of gravitational radiation. PhD Thesis, University of Glasgow.
- Strain, K. A., and Meers, B. J. (1991). *Phys. Rev. Lett.* **66**, 1391.
- Tsubono, K., and Moriwaki, S. (1992). *Jpn J. Appl. Phys.* **31**, 1241.
- Vinet, J. Y., Meers, B., Man, C. N., and Brillat, A. (1988). *Phys. Rev. D* **38**, 433.
- Vogt, R. E. (1991). Proc. 6th Marcel Grossmann Meeting on General Relativity, Kyoto (Eds H. Sato and T. Nakamura), p. 244 (World Scientific: Singapore).
- Weigarten, K. J., Rodwell, M. J. W., and Bloom, D. M. (1988). *IEEE J. Quant. Electron.* **24**, 198.
- Weiss, R. (1972). MIT Research Laboratory of Electronics Report No. 105, 54 (unpublished).
- Xiao, M., Wu, L.-A., and Kimble, H. J. (1987). *Phys. Rev. Lett.* **59**, 278.
- Yariv, A. (1985). In 'Optical Electronics' 3rd edn, §6.9 (CBS College Publishing: New York).
- Yoshino, T., Nara, M., Mnatzakanian, S., Lee, B. S., and Strand, T. C. (1987). *Appl. Opt.* **26**, 892.

